Simulation of facet heating in high power red lasers

J. M.G. Tijero*[a], H. Odriozola[a], I. Esquivias[a], A. Martin-Minguez[a], L. Borruel[a], A. Gomez-Iglesias[b], M. Reufer[b], M. Bou-Sanayeh[b], P. Brick[b], N. Linder[b], M. Ziegler[c] and J. W. Tomm[c]
[a] Universidad Politécnica de Madrid, ETSI Telecomunicación, Madrid 28040, Spain
[b] OSRAM Opto Semiconductors GmbH, Regensburg 93055, Germany
[c] Max-Born-Institut, Max-Born-Str. 2 A, 12489 Berlin, Germany

ABSTRACT

A two-dimensional self-consistent laser model has been used for the simulation of the facet heating of red emitting AlGaInP lasers. It solves in the steady-state the complete semiconductor optoelectronic and thermal equations in the epitaxial and longitudinal directions and takes into account the population of different conduction band valleys. The model considers the possibility of two independent mechanisms contributing to the facet heating: recombination at surface traps and optical absorption at the facet. The simulation parameters have been calibrated by comparison with measurements of the temperature dependence of the threshold current and slope efficiency of broad-area lasers. Facet temperature has been measured by micro-Raman spectrometry in devices with standard and non absorbing mirrors evidencing an effective decrease of the facet heating due to the non absorbing mirrors. A good agreement between experimental values and calculations is obtained for both devices when a certain amount of surface traps and optical absorption is assumed. A simulation analysis of the effect of non absorbing mirrors in the reduction of facet heating in terms of temperature, carrier density, material gain and Shockly-Read-Hall recombination rate profiles is provided.

Keywords: Laser simulation, facet heating, non absorbing mirror, red laser, high power lasers

1. INTRODUCTION

Facets are the hottest regions in the regular operation of laser diodes and therefore the places where the thermal degradation processes limiting the reliability of high power laser diodes originate[1-6]. Facet heating is the result of a complex mechanism which ultimate origins are commonly attributed to the boundary character of the facet giving rise to a concentration of non-radiative defects higher than in the bulk. These defects, acting as non-radiative recombination traps and/or reabsorbing centers are recognized as the seeds of the facet heating process[1-3, 7-8]. The problem is more severe in AlGaInP red lasers than in the AlGaAs near infrared devices due to the comparatively high photon energy and thermal and electrical resistivities of the AlGaInP material system leading to a Joule heating stronger than in AlGaAs devices[5, 9-10]. In the attempts to mitigate facet heating, several strategies leading to the formation of Non-Absorbing Mirrors (NAM) by enlarging the band-gap of the active layer in a thin section close to the facet have demonstrated to improve the reliability of the lasers[11-14].

Facet heating has been addressed experimentally in many works mainly aimed at the description and understanding of the process leading to laser failure by Catastrophic Optical Mirror Damage (COMD)[3,5-6,15-18]. However the advances are hindered by the local character of the process, the close proximity of the bulk and surface regions in which temperature has to be discriminated, the rapid run away process leading to COMD and the destructive character of some experimental tests. These limitations make convenient a complementary simulation approach which can enlighten the physical mechanisms underlying the process, provide design guidelines to alleviate the problem and assess some of the proposed mitigation strategies.

* jm.g.tijero@upm.es; phone 34 91 3366569; fax 34 91 3366554

Since the first attempts of modelling facet heating[1] several analytical approaches have been considered[1-2,19-21]. Although these approaches have provided qualitative insight into the physics of the phenomenon they have also important limitations. Among them, the high number of assumptions required to solve analytically the set of equations which may obscure a detailed quantitative analysis, the lack of consistency between the optoelectronic and thermal equations, and the fact that, consequently, they cannot handle self-consistently the entire device, thereby lacking in a proper analysis of the effects of distant regions in the facet heating.

Therefore, self-consistent simulation tools enabling an integral simulation of the entire device[22-23] in conjunction with experimental tests are required in order to analyze quantitatively the effect of design parameters on the facet heating and provide integral designs of laser diodes with reduced facet heating and improved reliability.

The objective of this paper is to show how a self-consistent simulation tool, conveniently calibrated and backed with experimental results can be used, in conjunction with experimental work, for the analysis of the facet heating of AlGaInP red lasers and its mitigation by means of NAM . We use a two-dimensional (2D) self-consistent electro-optical and thermal model based on the model by Romero et al[24]. The model considers the complete bipolar semiconductor equations and takes into account the population of different conduction band valleys. Simulations are compared with micro-Raman (μR) measurements of the facet temperature of devices with standard and NAM facets.

The paper is organized as follows: In section 2 a summary of the main characteristics of the model with special emphasis in the specificities required for the simulation of red lasers is presented. Details of the simulated and measured devices and the procedure for the calibration of the simulation tool, as well as a brief description of the μR technique are provided in section 3. Section 4 is devoted to the comparison and analysis of the experimental and simulation results on facet heating of devices with standard and NAM facets. Section 5 deals with the simulation analysis of the effect of NAM on facet heating, in terms of temperature, carrier density, material gain and heat source density profiles in the cavity axis. Finally, the main conclusions are summarized in section 6.

2. THEORETICAL MODEL

The model that we have used is an upgraded version of a previous model initially developed for infrared lasers and detailed elsewhere[24]. The model has been conveniently modified to incorporate the specificities of AlGaInP lasers, in particular those arising from the proximity of the X and Γ valleys in the conduction band profile of AlGaInP alloys with intermediate Al content. We will provide here only a brief account of the main characteristics of the general model and a few general comments on the required modifications for the simulation of red emitting lasers. A detailed description of the upgraded model will be published elsewhere.

The model solves self-consistently the basic optical, electrical and thermal equations of a Fabry-Perot Quantum Well (QW) laser in two dimensions: the longitudinal direction (z-axis) and the direction of the current injection (vertical direction or y-axis). The lateral dimension is not considered and the model assumes uniform values of all the variables in this direction. The optoelectronic equations are solved only in the epitaxial layers (n- and p- contacts, cladding and confinement layers and QW regions) while the thermal equations are solved along the complete structure, including metals and substrate. The main advantages of our 2D approach are: i) since the laser is driven at constant voltage the current density distribution can be readily calculated and there is not need of assuming it, ii) the temperature distribution is calculated self-consistently with other local variables, iii) the temperature dependence of material parameters such as band gap or recombination coefficients is taken into account.

As optoelectronic equations the model solves the Poison equation, the continuity equations for electron and holes and the photon rate equation. The charges included in the Poisson equation are those arising from unconfined carriers and totally ionized impurities in all the epilayers, together with the confined carriers in the QW. Boltzmann statistics is considered for the bulk carriers and Fermi-Dirac for the confined carriers. In the QW both, bulk carriers and confined carriers are considered. The interaction between them is described by a carrier capture/escape model[25]. Material gain spectra are calculated using standard formulae[26]. In order to reduce computing time we have used a parabolic approximation to the valence band E-k diagrams. Non radiative recombination includes Shockly-Read-Hall (SRH) at both, bulk traps and surface traps. A negligible Auger recombination has been considered for the relatively high band gap material system AlGaInP. In the bulk regions spontaneous recombination is calculated using a temperature dependent bimolecular coefficient. Only the contribution of electrons populating the Γ valley has been considered. The standard formula

mentioned above is used for the calculation of the spontaneous recombination in the QW region. The distribution of photons in the vertical direction is calculated by solving the waveguide equation with the index profile of the passive structure. Along the longitudinal direction the photon density is obtained by solving the beam propagation equation assuming a constant modal gain which is calculated from the local material gain and the photon density profile by a two-dimensional integral. In the photon rate equation losses from mirrors, scattering and free carriers are considered, the last being calculated from the overlap integral of the photon and carrier density profiles.

We have considered surface traps at the facets of the QW regions. These traps give rise to a surface charge density in the Poisson equation and to a surface recombination term in the continuity equations. This term is calculated from the two-dimensional version of the SRH formula. Temperature distribution is calculated by solving the two-dimensional heat flow equation. Besides the usual sources, we have also considered two heat sources at the facets: the SRH recombination at the surface traps and some optical absorption at the AR facet. Therefore, the model considers two independent facet heating mechanisms: surface trap recombination and optical absorption. For the first mechanism, the model allows two spatial distributions of surface traps: surface distribution characterized by a surface density, and traps diffused deeper into the QW with a Gaussian profile characterized by a diffusion length and a maximum volume density. The heating by optical absorption is modelled by assuming that a fraction of the radiation leaving the cavity is absorbed at the facet, out of the laser cavity (i.e., non affecting the modal losses). The corresponding heat source is proportional to the output power and its spatial distribution corresponds to the vertical profile of the optical mode.

The boundary conditions for the heat flow equation are: negligible heat flow at the substrate and mirror interfaces and a heat flow towards the heat sink controlled by an effective thermal resistance at the heat sink determined by comparison with experimental results.

The complex conduction band structure of the AlGaInP red lasers posses some additional problems to the standard calculation of carrier and current densities in the confinement layers where the Γ and X valleys lay close together and therefore both are significantly populated at the laser operation conditions. An approach inspired in Ref [27] has been followed in order to account for both, the electron density and the electron current density using the standard formalism with a redefinition of an *equivalent effective mass* and an *equivalent mobility of electrons* which are functions of the effective masses and mobilities in both valleys, the energy minima of the valleys and the temperature.

For the resolution of the non-linear system of differential equations, a two-dimensional grid was considered and the equation system was discretized using the standard finite difference method. Special care was devoted to the selection of an adequate mesh at the surface and boundary regions where the abrupt variations of some parameters makes it specially critic. All the results were consistently checked by analyzing their dependence on the choice of mesh and convergence criteria.

The model can be used for the simulation of the effect of NAM. A NAM is modelled by assuming that the QW material is replaced in the vicinity of the facet by a larger band-gap, and otherwise identical, material. The band alignment of the new material keeps the same ratio between the conduction and valence band offsets that the original material.

3. EXPERIMENTAL

The simulated devices are Broad-Area (BA) red-emitting AlGaInP lasers grown by metal-organic vapour phase epitaxy on *n*-GaAs substrates. The active region consists of a single QW layer designed to emit at around 640 nm. The active layer is confined by AlGaInP waveguide and cladding layers. The front and rear facet of the standard devices are coated such that the resulting reflectivities are $R_1 = 0.10$ and $R_2 = 0.95$, respectively. The devices are mounted *p*-side down on standard copper C-mount heat sink.

Since there are some unknown parameters and some other material parameters that depend on the fabrication process, the model requires a fitting procedure with experimental results. 1200 μm long and 100 μm wide BA devices were used for this procedure. The experimental values of the threshold current I_{th} and the slope efficiency η_s as a function of the temperature in pulsed regime were fitted to those obtained from the simulation of the P-I characteristics under isothermal conditions as a function of the temperature. The fitting parameters were the bulk trap density in the QW, confining and cladding layers, and the electron and hole capture times. The values of these fitting parameters were kept constant in the subsequent 2D simulations of facet heating. As an illustrative example Fig. 1 shows the comparison between the experimental pulsed P-I and the simulated characteristics assuming a high density of traps in the p cladding layer.

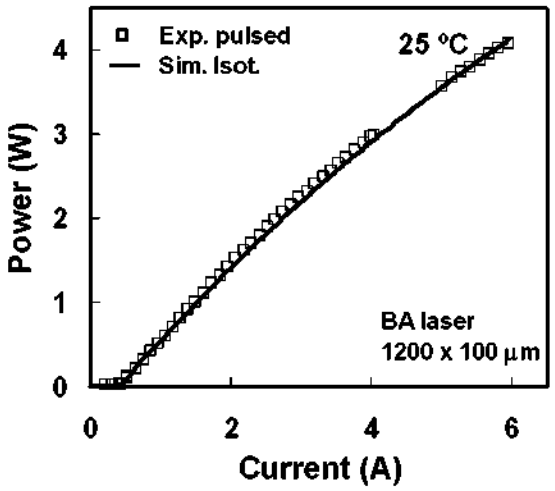

Figure 1. Fitting of the experimental (open squares) and simulated (solid line) P-I curves of a 1200 x 100 µm BA laser. The experimental curve was recorded in pulsed regime and the simulation was done under isothermal conditions, both at 25 °C.

Facet temperatures were measured by micro-Raman (µR) spectrometry; see, e.g., ref [28]. The excitation source was the 488 nm line of an Ar-ion laser focussed on the front facet on a spot which diameter, $Ø_{1/e}$ ~1 µm, covers the active region. The excitation power was about 1 mW and the estimated 'information depth' was about 100 nm. Raman spectra were recorded with a Dilor x-y-µR-spectrometer. Facet temperatures were determined by the shift of the Stokes line of the AlP-like LO-phonon generated at the surface and were cross-checked by an analysis of the intensity ratio of the Stokes and anti-Stokes lines. The estimated accuracy of these measurements is ±10 K. Measurements were done at a stabilized heat-sink temperature of 25 °C.

4. SIMULATION AND EXPERIMENTAL RESULTS. COMPARISON

The 2D simulation tool predicts different facet heating as a function of the driving current depending on the facet heating mechanism considered, namely, optical absorption and surface trap recombination, and depending on the amount of surface traps and optical absorption at the facet considered in each case. Figs. 2-4 show illustrative examples for a variety of cases with different contributions of both mechanisms. The simulated device was in all the cases a 1200x50 µm BA laser. The most significant difference is the heating at threshold when surface traps are considered (Figs. 3-4). This heating is obviously absent when only optical absorption is considered (Fig. 2).

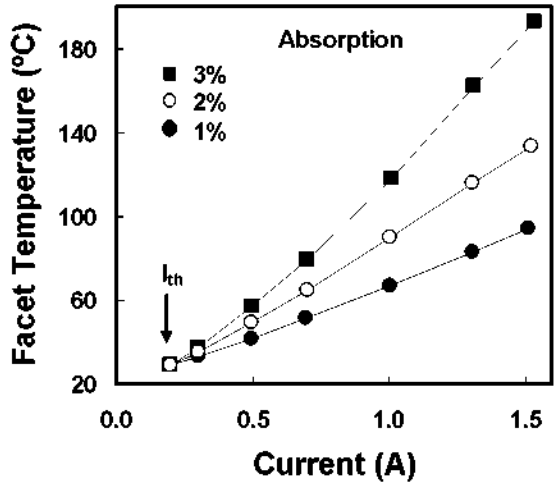

Figure 2. Simulated facet temperature as a function of the injection current of a 1200x50 µm BA laser when an optical absorption of 1% (solid circles), 2% (open circles) and 3% (solid squares) is assumed as facet heating source.

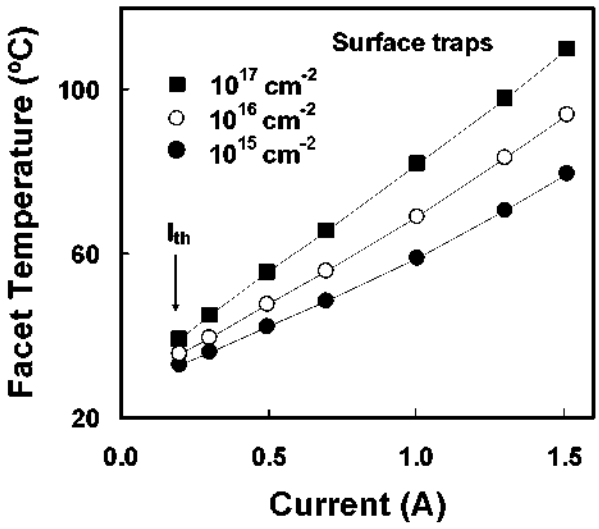

Figure 3. Simulated facet temperature as a function of the injection current of a 1200x50 μm BA laser when heating by recombination at surface traps is assumed. The surface trap densities were 10^{15}cm^{-2} (solid circles), 10^{16}cm^{-2} (open circles) and 10^{17}cm^{-2} (solid squares).

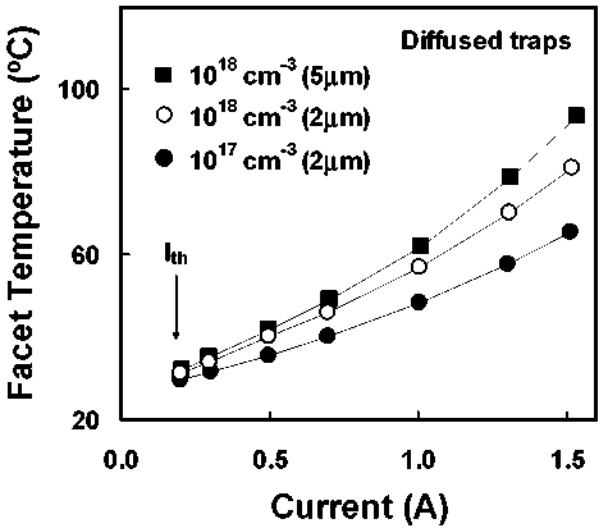

Figure 4. Simulated facet temperature as a function of the injection current of a 1200x50 μm BA laser when heating by recombination at diffused surface traps is assumed. The trap densities were 10^{17}cm^{-3} and 10^{18}cm^{-3} with diffusion length 2 μm (solid and open circles, respectively) and 10^{18}cm^{-3} with diffusion length 5 μm (solid squares).

For comparison purposes, the facet temperature of the 1200x50 μm BA device considered in Figs. 2-4 was measured by μR spectrometry. The measured temperature as a function of the driving current is plotted in Fig. 5, together with a minimum square linear fitting of the data for $I > I_{th}$ (slope ~ 105 °C/A). The simulated values that best fit the experimental results are also plotted. The fitting could not be achieved by assuming only surface and/or diffused traps, but required the contribution of some additional heating by optical absorption at the facet. The values of the absorption, and the density of surface and diffused traps for this fitting were 1.2%, 4 x 10^{15} cm^{-2} and 10^{18} cm^{-3} (2 μm diffusion length), respectively.

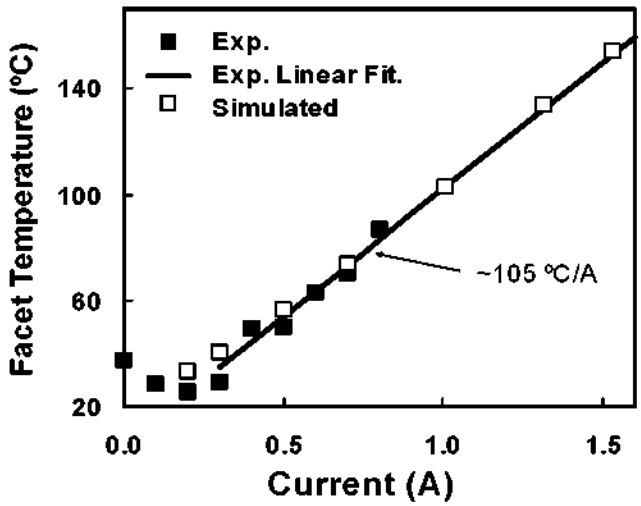

Figure 5. Experimental (solid squares) and simulated (open squares) facet temperature as a function of the injection current of a laser with standard mirrors. The straight line is the linear fitting of the experimental values for $I > I_{th}$.

The facet temperature of a device from the same batch was also measured after processing its front facet as a Non Absorbing Mirror (NAM) by increasing the QW material band-gap as to make it transparent to the laser radiation in a thin section close to the facet. Fig. 6 shows the measured facet temperature of the device with NAM together with the minimum square linear fitting of the data for $I > I_{th}$ (slope ~ 88 °C/A). It is worth to mention here that the P-I characteristics of the NAM devices in pulsed regime (non shown) showed a significant increase of the maximum attainable power with respect to the devices with standard mirror. The facet temperature of the device with NAM was also simulated. In the simulation we used the same densities of surface and diffused traps and optical absorption at the facet that best fitted the measured facet heating of the device with standard mirror, and the same band gap increase ΔE_g resulting after the NAM processing extended along a section next to the front facet of the same thickness Δz as the processed section. The simulation results are also plotted in Fig. 6. A remarkable agreement between the simulated temperature and the linear fitting of the measured temperature is apparent for a large range of injection current.

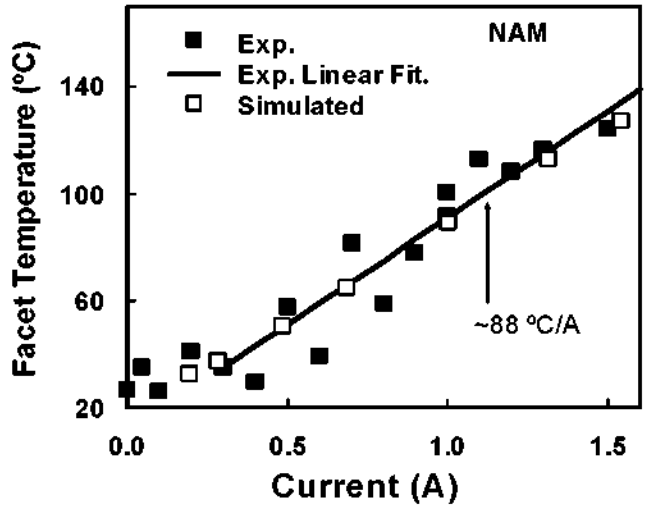

Figure 6. Experimental (solid squares) and simulated (open squares) facet temperature as a function of the injection current of a laser with NAM. The straight line is the linear fitting of the experimental values for $I > I_{th}$.

Examining together Figs. 5 and 6 two important facts are apparent: First, an adequate processing of the front facet as NAM is readily efficient for the overall reduction of the facet temperature. This clear experimental evidence is also

corroborated at least qualitatively by simulations and indicates that surface traps are at least partially responsible of the facet heating of these devices. Second, simulation results agree with experimental findings both prior and after NAM processing when a certain amount of surface and diffused traps as well as some optical absorption at the facet are admitted to contribute to facet heating. The fact that the agreement between the simulated facet temperature and the linear fitting of the experimental values for the device with NAM was achieved straightforwardly by using the same trap densities and optical absorption that best fitted the measured facet heating of the device with standard mirror points to the internal consistency of the simulation results. Furthermore, it gives support to the use of the simulation tool for the analysis of the effect of NAM in the facet heating reduction to be done in the next section. Nevertheless, the relatively high number of fitting parameters (optical absorption, density of surface and diffused traps, diffusion length...) on the one hand, and the inherently low accuracy of the μR spectrometry technique (~ 10 K) on the other hand preclude any definite conclusion on the specific contribution of each mechanism to the facet heating.

5. SIMULATION ANALYSIS OF THE EFFECT OF NAM

Fig. 7 shows the simulated facet temperature of the 1200x50 μm BA laser as a function of the energy shift of the NAM, ΔE_g. The simulations were done for a common bias current I = 1.3 A and the thickness of the NAM was Δz = 20 μm. The same amounts of traps and optical absorption at the facet that best fitted the experimental facet heating were considered. The simulations predict a significant heating reduction for ΔE_g higher than 20 meV.

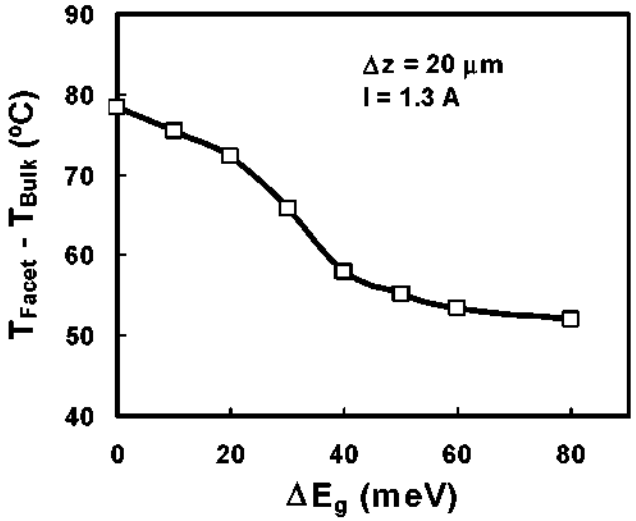

Figure 7. Simulated QW temperature difference between the facet and the bulk as a function of the QW energy shift of the NAM. The temperatures were calculated for and injection I = 1.3 A and a thickness of the inter-diffusion region Δz = 20 μm.

The simulation tool was used for a detailed analysis of the effect of NAM in the decrease of the facet heating. The simulated device was again the 1200x50 μm BA laser. The NAM parameters in the simulations were Δz = 20 μm and ΔE_g = 80 meV and the bias current was I = 1.3 A in all the cases.

Fig. 8 shows the simulated QW temperature profiles along the cavity axis in a region close to the facet for the devices with standard mirror and with NAM. The increasing temperature profile of the device with standard mirror has been attributed to the following mechanism [Romero 00]. The recombination of the carriers at the traps gives rise to an increase of the surface heat sources and a decreasing carrier density profile. As a consequence of this carrier depletion the material gain drops eventually below zero and the material becomes absorbing (see Fig. 9). Then, the absorbed photons create new carriers which partially balance the depletion but in turn recombine generating additional heating. In addition, the rise of the temperature near the surface (also due in this case to the optical absorption mechanism) induces a higher population of the bands near the surface. This is due, on the one hand, to the thermal band-gap shrinkage and, on the other hand, to the fact that the quasi-Fermi level separation has to keep approximately the same value at the surface and in the bulk since the entire device, surface and bulk, is driven at constant voltage along the cavity axis. These

additional carriers are also available for recombination generating more heating. As a result of the entire process the carrier density profile (non shown) exhibits a sharp decrease in the region close to the facet and the QW temperature rises as shown in Fig. 8.

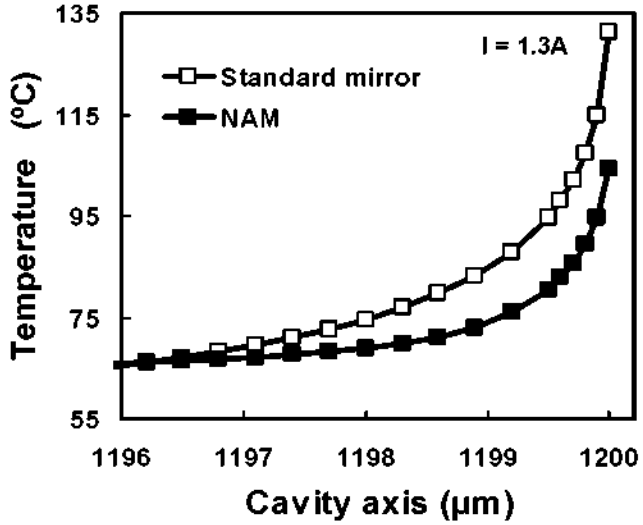

Figure 8. Simulated profile of the QW temperature along the cavity axis in the vicinity of the facet. Open squares: device with standard mirror. Solid squares: device with NAM. The injection current is I = 1.3 A for both devices.

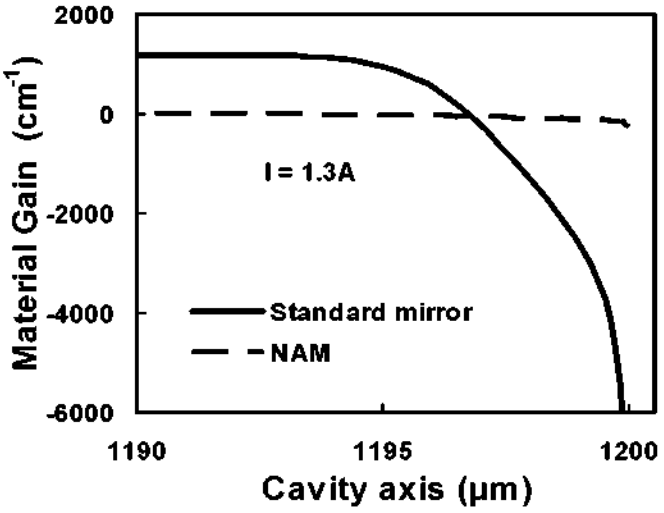

Figure 9. Simulated profiles of the QW material gain along the cavity axis in the vicinity of the facet. Solid line: device with standard mirror. Dashed line: device with NAM. The injection current is I = 1.3 A for both devices.

The role of the NAM is to mitigate the facet temperature increase by avoiding the generation of new carriers by photon absorption in the NAM region. The QW material gain profiles of the devices with standard mirror and NAM have been plotted in Fig. 9. The gain of the NAM device vanishes in the NAM region due to the increase of the QW band-gap. Therefore, the material becomes transparent to the laser photons, thus avoiding the heating effects of the photo-generated carriers described above. This finally results in the reduced facet heating shown in Fig. 8. This interpretation is further supported by Figs. 10 and 11. In Fig. 10 the profiles along the cavity axis of the SRH recombination rate have been plotted in both cases. As expected, the SRH recombination rate is significantly lower in the case of the NAM device and consequently a lower heating from this source is expected. Finally, Fig. 11 shows comparatively the profiles of the heat

source density in the epitaxial (vertical) direction at a section close to the surface. Again, the reduced heat source density in the QW region in the case of the NAM device gives additional support to the interpretation of the role of the NAM pictured in this section.

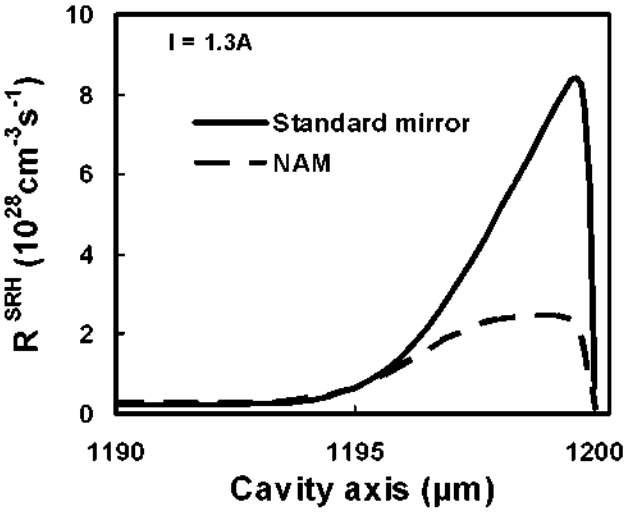

Figure 10. Simulated profiles of the SRH recombination rate along the cavity axis in the vicinity of the facet. Solid line: device with standard mirror. Dashed line: device with NAM. The injection current is I = 1.3 A for both devices.

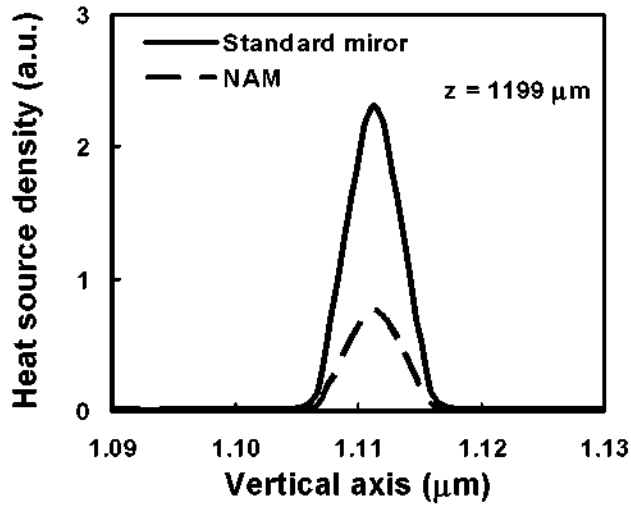

Figure 11. Vertical profiles of the density of heat sources at a section close to the facet (z = 1199 mm). Solid line: device with standard mirror. Dashed line: device with NAM. The injection current is I = 1.3 A for both devices.

6. CONCLUSIONS

The facet temperature of BA AlGaInP red emitting lasers has been calculated with a self-consistent two-dimensional simulation tool and measured by μ-Raman spectrometry in devices with standard mirrors and NAM. A good agreement between calculations and measurements has been found when the simulation tool is properly calibrated with experimental results and both surface trap recombination and optical absorption are assumed. The use of NAM has been demonstrated as an efficient means for the effective reduction of facet heating in these lasers. When used in conjunction with experimental work, the simulation tool has proved its usefulness for the analysis of facet heating and the positive effect on it of the use of NAM.

ACKNOWLEDGMENTS

The authors gratefully acknowledge the support of the European Commission through the IST project n°2005-035266, WWW.BRIGHTER.EU, and of the MEC (Spain) through projects TEC2006-13887 and TEC2007-29619-E.

REFERENCES

[1] Henry, C. H., Petroff, P. M., Logan, R. A. and Merritt, F. R., "Catastrophic damage of $Al_xGa_{1-x}As$ double – heterostructure laser materials", J. Appl. Phys. 50, 3721-3732 (1979).
[2] Schatz, R. and Bethea, C. G., "Steady state model for facet heating leading to thermal runaway in semiconductor lasers", J. Appl. Phys. 76, 2509-2521 (1994).
[3] Tang, W. C., Rosen, H. J., Vettiger P. and Webb, D. J., "Raman microprobe study of the time development of AlGaAs single quantum well laser facet temperature on route to catastrophic breakdown", Appl. Phys. Lett. 58, 557-559 (1991).
[4] Tien, Q., Weik, F., Tomm, J. W., Sumpf, B., Zorn, M., Zeimer, U. and Erbert, G., "Thermal properties and degradation behavior of red-emitting high-power diode lasers" Appl. Phys. Lett. 89, 181112, (2006).
[5] Bou-Sanayeh, M., Brick, P., Schmid, W., Mayer, B., Müller, M., Reufer, M., Streubel, K., Tomm, J. W. and Bacher, G., "Temperature-power dependence of catastrophic optical damage in AlGaInP laser diodes" Appl. Phys. Lett. 91, 041115 (2007).
[6] Ziegler, M., Tomm, J. W., Elsaesser, T., Matthiesen, C., Bou Sanayeh M. and Brick, P., "Real-time thermal imaging of catastrophic optical damage in red-emitting high-power diode lasers" Appl. Phys. Lett. 92, 103514 (2008).
[7] Tu, L. W., Schubert, E.F., Hong, M. and Zydzik, G. J., "In-vacuum cleaving and coating of semiconductor laser facets using thin silicon and a dielectric", J. Appl. Phys. 80(11), 6448-6451 (1996).
[8] Yeoh, T. S., Chaney, J. A., Leung, M. S., Ives, N. A., Feinberg, Z. D., Ho, J. G., and Wen, J., "Three-dimensional failure analysis of high power semiconductor laser diodes operated in vacuum", J. Appl. Phys. 102, 123104 (2007).
[9] Fujii, H., Ueno, Y. and Endo, K., "Effect of thermal resistivity on the catastrophic optical damage power density of AlGaInP laser diodes", Appl. Phys. Lett. 62, 2114-2116 (1993).
[10] Bou Sanayeh, M., Jaeger, A., Schmid, W., Tautz, S., Brick, P., Streubel, K. and Bacher, G., "Investigation of dark line defects induced by catastrophic optical damage in broad-area AlGaInP laser diodes", Appl. Phys. Lett. 89, 101111 (2006).
[11] Piva, P. G., Fafard, S., Dion, M., Buchanan, M., Charbonneau, S., Goldberg, R. D. and Mitchell, I. V., "Reduction of InGaAs/GaAs laser facet temperatures by band gap shifted extended cavities"", Appl. Phys. Lett. 70(13), 1662-1664 (1997).
[12] Hiramoto, K., Sagawa, M., Kikawa, T. and Tsuji S., "High-power and highly reliable operation of Al-free InGaAs-InGaAsP 0.98-μm lasers with a window structure fabricated by Si ion implantation," IEEE J. Sel. Topics Quantum Electron., 5(3), 817–820 (1999).
[13] Yamada, Y., Yamada, Y., Fujimoto T. and Uchida, K., "High power and highly reliable 980 nm lasers with window structure using impurity free vacancy disordering," Proc. SPIE 5738, 40–46 (2005).
[14] Taniguchi, H., Ishii, H., Minato, R., Ohki, Y., Namegaya, T. and Kasukawa, A., "25-W 915-nm lasers with window structure fabricated by Impurity-Free Vacancy Disordering (IFVD)", IEEE J. Sel. Topics Quantum Electron. 13(5), 1176–1179 (2007).
[15] Ueda, O., "Reliability and Degradation of III-V Optical Devices", Artech House, Boston (1996).
[16] Snyder, C. W., Lee, J. W., Hull, R. and Logan R. A., "Catastrophic degradation lines at the facet of InGaAsP/InP lasers investigated by transmission electron microscopy", Appl. Phys. Lett. 67(4), 488-490 (1995).
[17] Park, K. H., Lee, J. K., Jang, D. H., Cho, H. S., Park, C. S., Pyun, K. E., Jeong, J. Y., Nahm, S. and Jeong J., "Characterization of catastrophic optical damage in Al-free InGaAs/InGaP 0.98 μm high-power lasers," Appl. Phys. Lett. 73(18), 2567–2569 (1998).
[18] Ziegler, M., Tomm, J. W., Reeber, D., Elsaesser, T., Zeimer, U., Larsen, H. E., Petersen P. M. and Andersen, P. E., "Catastrophic optical mirror damage in diode lasers monitored during single pulse operation," Appl. Phys. Lett. 94(19), 191101 (2009).
[19] Yoo, J. S., Lee H. H. and Zory, P., "Temperature rise at mirror facet of CW semiconductor lasers", IEEE J. Quantum Electron. 28, 635-639 (1992).
[20] Chen G. and Tien, C. L., "Facet heating of quantum well lasers", J. Appl. Phys. 74, 2167-2174 (1993).

[21] Nakwaski, W., "Thermal model of the catastrophic degradation of high-powe strip geometry GaAs/(AlGa)As double-heterostructure diode lasers", J. Appl. Phys. 67, 1659-1668 (1990).
[22] Menzel, U., "Self-consistent calculation of facet heating in asymmetrically coated edge emitting diode lasers" Sem. Sci.Tech. 13, 265-276 (1998).
[23] Romo, G., Smy, T., Walkey D. and Reid, B., "Modeling facet heating in ridge lasers", Microelectron Reliab. 43, 99-110 (2003).
[24] Romero, B., Batko, G., Arias J., Borruel, L., Esquivias, I. and Gómez-Alcalá, R., "Modeling of facet heating in high power laser diodes" Proc. SPIE 3889, 96-106 (2000).
[25] Borruel, L., Arias, J., Romero B. and Esquivias, I., "Incorporation of carrier capture and escape processes into a self-consistent cw model for Quantum Well lasers," Microelectronics Journal, 34, 675-677 (2003).
[26] Coldren L. A. and Corzine, S. W., "Diode Lasers and Photonic Integrated Circuits," Wiley, New York (1995).
[27] Sutherland, J. E., and Hauser, J. R., "A computer analysis of heterojunction and graded composition solar cells," IEEE Trans. Electron Devices, 24(4), 363-372 (1977).
[28] Tomm, J. W., Thamm, E., Barwolff, A., Elsaesser, T., Luft, J., Baeumler, M., Mueller, S., Jantz, W., Rechenberg, I. and Erbert, G., "Facet degradation of high-power diode laser arrays" Applied Physics a-Materials Science & Processing 70(4), 377-381 (2000).